

# Impact-parameter-dependent solutions to the Balitsky-Kovchegov equation at next-to-leading order

J. Cepila, J. G. Contreras, M. Matas, and M. Vaculciak\*

*Czech Technical University in Prague*

arXiv:2412.08571v1 [hep-ph] 11 Dec 2024

# Abstract

A stable numerical solution of the impact-parameter-dependent next-to-leading order Balitsky-Kovchegov equation is presented for the first time. The rapidity evolution of the dipole amplitude is discussed in detail. Dipole amplitude properties, such as the evolution speed or anomalous dimension behaviour, are studied as a function of the impact parameter and the dipole size and compared to solutions of the impact-parameter-dependent leading-order Balitsky-Kovchegov equation with the collinearly improved kernel. The next-to-leading evolution also strongly suppresses the Coulomb tails compared to the collinearly improved and leading order solutions.

## I. INTRODUCTION

Precise deep-inelastic scattering data from electron–proton collisions at the HERA accelerator show that the gluon content of the proton grows as a power law for decreasing values of Bjorken- $x$  [1]. This behaviour cannot continue unchecked to arbitrarily small Bjorken- $x$ , or high energy, correspondingly, as it would violate basic properties of quantum chromodynamics (QCD). It was predicted long ago, that the growth of the gluon distribution in hadrons would be tamed by the recombination of gluons [2, 3]. This phenomenon is called *saturation* and its experimental confirmation is an important research topic in theoretical studies of perturbative QCD (see e.g. Ref. [4] for a recent review) as well as in the experimental arena. Here the LHC has recently provided several interesting measurements at high energies [5–7], and the community is eagerly awaiting the start of operations of the Electron–Ion Collider, which is currently in construction and features the search for gluon saturation as one of its pillars [8, 9].

An appropriate framework to study the high-energy limit of QCD is the dipole picture [10] where a quark-antiquark pair forms a colour dipole that interacts with the colour fields of the probed target. In the case of photon-induced interactions, such dipole is provided by a fluctuation of a photon into a quark-antiquark state. In the eikonal approximation, the propagation of the dipole through the target can be described in the Colour Glass Condensate approach, see e.g. Ref. [11], giving rise to the B-JIMWLK equations [12–20]. In the limit of a large number of colours, these equations reduce to the Balitsky-Kovchegov

---

\* matej.vaculciak@fjfi.cvut.cz

(BK) equation [12, 21, 22], which gives the evolution of the dipole amplitude  $N(Y, \vec{r}, \vec{b})$  in rapidity  $Y$ . The amplitude itself then describes the scattering of the incoming colour dipole of transverse size  $\vec{r}$  with a hadronic target located at a distance given by the impact parameter vector  $\vec{b}$ .

The original BK equation was computed at the leading order (LO). Later on, the running of the coupling constant was included in the BK formalism [23, 24] and the resulting equation was then used to successfully describe data from deep-inelastic scattering [25, 26]. In this last work, and most of those following it, the dipole amplitude was taken as depending only on rapidity and the size of the dipole  $r \equiv |\vec{r}|$ , that is  $N(Y, r)$ , representing the interaction of the dipole with an infinite homogeneous target. Other higher-order effects were computed by resumming the radiative corrections enhanced by large double transverse logarithms and including single-logarithmic corrections [27, 28]; the resulting collinearly improved (CI) BK equation, was again used to obtain a good description of deep-inelastic scattering data [28].

Two ingredients are needed to contrast the BK equation with data at next-to-leading order (NLO) precision: the computation of impact factors at NLO and the NLO BK equation. Regarding the former, there has been considerable advance in the last few years in computing NLO impact factors for different observables, see e.g. Refs. [29–35]. As for the latter, the NLO BK equation has been originally obtained in Ref. [36]. Solutions of the form  $N(Y, r)$  were studied numerically in Ref. [37], where it was found that this equation produced unphysical results. The problem was identified as the large double transverse logarithmic NLO corrections, which are present in the full NLO BK equation with a negative sign. A viable form of the NLO BK equation was presented in Ref. [38], where the  $N(Y, r)$  solutions were demonstrated to be stable, when including the resummation of single and double logarithms in a procedure akin to what was done at LO [27, 28].

The first attempt to include the dependence on the impact parameter in the dipole amplitude, interpreted physically as a target of finite size and with a profile in impact parameter, was presented in Ref. [39] where the original LO BK equation was studied. It was found that in this case the amplitude develops unhealthy Coulomb tails, a power-law growth of the amplitude with rapidity at large impact parameters. This behaviour was not physical and precluded the use of these solutions for phenomenology. A modified BK equation introducing a cutoff in the kernel as a proxy for kinematic constraints [40] was studied [41] and used to describe deep-inelastic scattering data [42] as well as diffractive

exclusive vector meson photoproduction [43]. However, the issue of unphysical Coulomb tails remained. A reasonable description of measurements was achieved only through the use of this cutoff and the addition of a non-perturbative contribution. With the aforementioned advent of the collinear corrections to the BK equation, our group studied impact-parameter dependent solutions of the form  $N(Y, r, b)$ , with  $b \equiv |\vec{b}|$ , to the CI BK equation, finding that the Coulomb tails are strongly suppressed in this case [44]. This allows for a good description of data without any extra ad hoc ingredients [44, 45]. The suppression of the Coulomb tails is explained by the fact that the CI kernel suppresses large daughter dipoles due to the time ordering imposed by the resummation. A similar suppression of power-law tails was found in a restricted range—that covers the region where measurement data exist—of the evolution in Ref. [46]. Recently, we extended this work to solutions of the form  $N(Y, r, b, \theta)$  with  $\theta$  representing the dipole orientation with respect to the impact parameter [47]. For those studies we used a variation of the BK equation with the evolution performed not in the rapidity of the projectile, but on the rapidity of the target [48].

In this article, we extend the results from Ref. [38] to the numerical study of solutions to the NLO BK equation by including the dependence on the size of the impact parameter in the dipole amplitude, i.e. we explore solutions of NLO BK of the form  $N(Y, r, b)$ . We find that the solutions are numerically stable. These NLO solutions have a slower evolution speed than the CI solutions. They exhibit a more stable anomalous dimension as rapidity increases than in the CI case. The NLO solutions also show a suppression of the power-law Coulomb tails, making them a viable ingredient for future comparison of observables with data.

The article is organised as follows: in Sec. II the BK equation at NLO and its leading order CI variant are briefly introduced, Sec. III introduces the method to obtain the stable numerical solutions of the BK equation, and Sec. IV presents the obtained dipole amplitudes and discusses their properties.

## II. THE BK EQUATION

### A. The BK equation at next-to-leading-order

Including an additional gluon contribution in the BK evolution, the projectile-rapidity next-to-leading order BK equation was derived in [36] and can be written as

$$\begin{aligned}
\partial_Y N_{xy} = & \int d^2z K_0 \left[ N_{xz} + N_{zy} - N_{xy} - N_{xz} N_{zy} \right] \\
& + \int d^2z d^2w K_1 \left[ N_{wy} + N_{zw} - N_{zy} - N_{xz} N_{zw} - N_{xz} N_{wy} \right. \\
& \quad \left. - N_{zw} N_{wy} + N_{xz} N_{zy} + N_{xz} N_{zw} N_{wy} \right] \\
& + \int d^2z d^2w K_2 \left[ N_{xw} - N_{xz} - N_{zy} N_{xw} + N_{xz} N_{zy} \right], \tag{1}
\end{aligned}$$

where  $N_a \equiv N(Y, r_a, b_a, \theta_a, \varphi_a)$ . Here  $a$  keeps track of the coordinates at the dipole ends, e.g.  $xy$ . Throughout this work, we assume an isotropic target, lifting the dependence of the scattering amplitude on the angle  $\varphi_a$ . Furthermore, we integrate out the angular orientation of the dipole with respect to the target  $\theta_a$ , leading to an amplitude that depends on the dipole size and impact parameter only  $N_a \equiv N(Y, r_a, b_a)$ . Figure 1, shows an example of the coordinates involved in the problem.

Resumming contributions from large transverse logarithms [28] and double logarithmic terms [27] the kernels take the form

$$K_0 = K_{\text{rc}} K_{\text{STL}} K_{\text{DLA}} - K_{\text{sub}} + K_{\text{fin}}, \tag{2}$$

where the LO running-coupling kernel is

$$K_{\text{rc}} = \frac{\alpha_s(r_{xy}) N_C}{2\pi^2} \left[ \frac{r_{xy}^2}{r_{xz}^2 r_{zy}^2} + \frac{1}{r_{xz}^2} \left( \frac{\alpha_s(r_{xz})}{\alpha_s(r_{zy})} - 1 \right) + \frac{1}{r_{zy}^2} \left( \frac{\alpha_s(r_{zy})}{\alpha_s(r_{xz})} - 1 \right) \right], \tag{3}$$

with  $N_C$  representing the number of colours. The part of the kernel present within the collinearly improved form of the BK equation is

$$K_{\text{DLA}} = \begin{cases} \frac{J_1(2\sqrt{\bar{\alpha}_s \rho^2})}{\sqrt{\bar{\alpha}_s \rho^2}} & \rho^2 > 0 \\ \frac{I_1(2\sqrt{-\bar{\alpha}_s \rho^2})}{\sqrt{-\bar{\alpha}_s \rho^2}} & \rho^2 < 0, \end{cases} \tag{4}$$

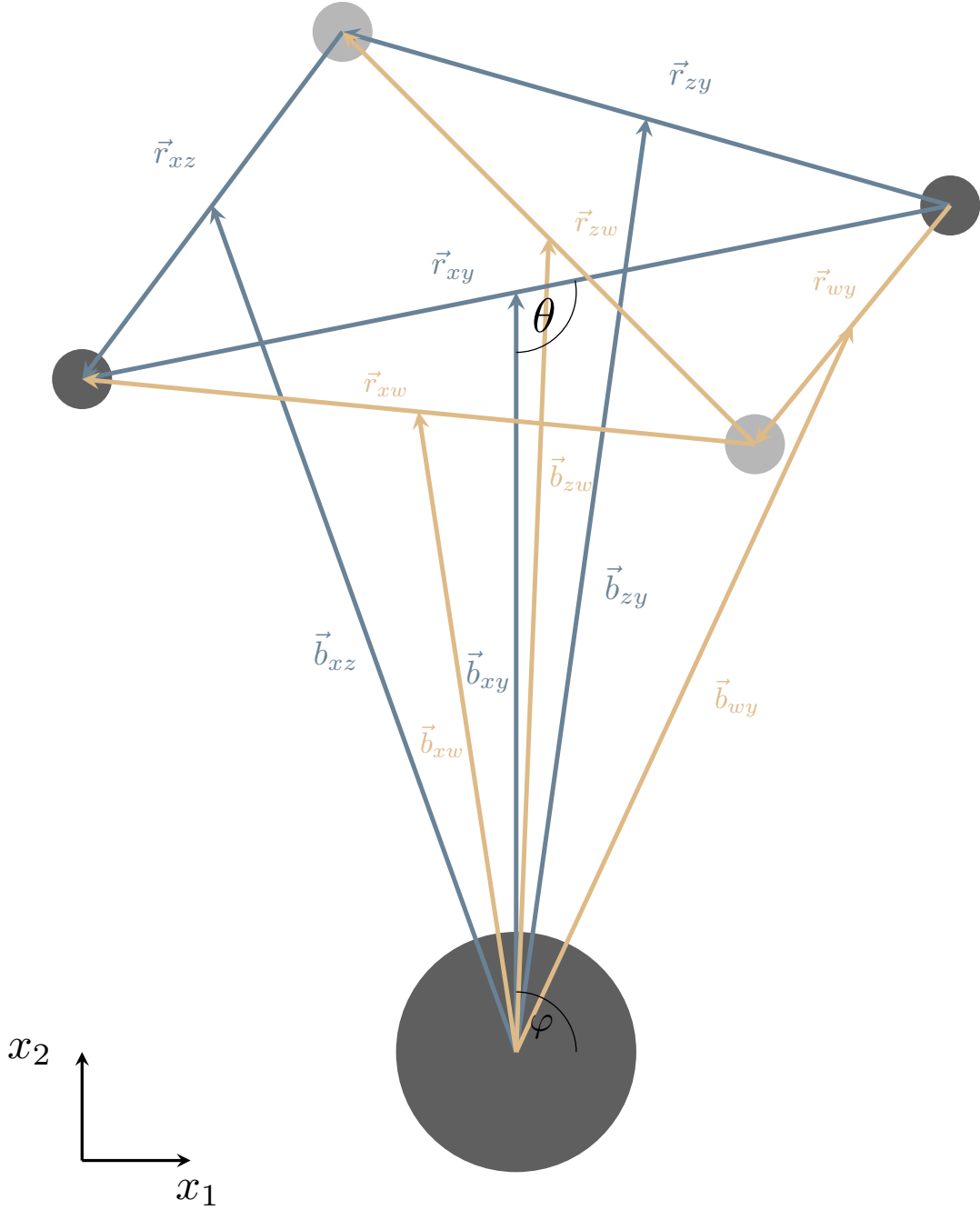


FIG. 1. The transversal structure of the mother and daughter dipoles within the next-to-leading evolution. The leading order contribution is highlighted in blue, while the additional gluonic emission and the associated dipoles are in orange. The angle  $\theta$  controls the tilting of the mother dipole with respect to the target and  $\varphi$  is the angle of the impact parameter. In this work, we assume an isotropic target and neglect the  $\theta$  dependence, so the scattering amplitude is a function of rapidity  $Y$ , dipole size  $r$ , and impact parameter  $b$  only.

where  $\rho^2 = \ln \frac{r_{xz}^2}{r_{xy}^2} \ln \frac{r_{zy}^2}{r_{xy}^2}$ . The remaining terms unique to the NLO evolution with a single-quark emission are

$$\begin{aligned} K_{\text{STL}} &= \exp \left[ -\bar{\alpha}_s A_1 \left| \ln \left( \frac{C_{\text{sub}} r_{xy}^2}{\min(r_{xz}^2, r_{zy}^2)} \right) \right| \right], \\ K_{\text{sub}} &= \frac{\bar{\alpha}_s}{2\pi} \left[ -\bar{\alpha}_s A_1 \left| \ln \left( \frac{C_{\text{sub}} r_{xy}^2}{\min(r_{xz}^2, r_{zy}^2)} \right) \right| \right] \frac{r_{xy}^2}{r_{xz}^2 r_{zy}^2}, \\ K_{\text{fin}} &= \frac{\bar{\alpha}_s^2}{8\pi} \frac{r_{xy}^2}{r_{xz}^2 r_{zy}^2} \left( \frac{67}{9} - \frac{\pi^2}{3} - \frac{10n_f}{9N_C} \right), \end{aligned} \quad (5)$$

where  $A_1 = \frac{11}{12}$ ,  $C_{\text{sub}} = 0.65$ ,  $n_f$  represents the number of active flavours and  $\bar{\alpha}_s = \frac{N_C}{\pi} \alpha(\min(r_{xy}, r_{xz}, r_{zy}))$ . The parts of the kernel responsible for a two-gluon emission represented by a double integral over  $dz$  and  $dw$  in the evolution are

$$\begin{aligned} K_1 &= \frac{\alpha_s^2(r_{xy}) N_C^2}{8\pi^4} \left[ -\frac{2}{r_{zw}^4} \left( \frac{r_{xz}^2 r_{wy}^2 + r_{xw}^2 r_{zy}^2 - 4r_{xy}^2 r_{zw}^2}{r_{zw}^4 (r_{xz}^2 r_{wy}^2 - r_{xw}^2 r_{zy}^2)} + \right. \right. \\ &\quad \left. \left. + \frac{r_{xy}^4}{r_{xz}^2 r_{wy}^2 (r_{xz}^2 r_{wy}^2 - r_{xw}^2 r_{zy}^2)} + \frac{r_{xy}^2}{r_{xz}^2 r_{wy}^2 r_{zw}^2} \right) \ln \frac{r_{xz}^2 r_{wy}^2}{r_{xw}^2 r_{zy}^2} \right], \end{aligned} \quad (6)$$

and

$$K_2 = \frac{n_f N_C \alpha_s^2(r_{xy})}{8\pi^4} \left[ \frac{2}{r_{zw}^4} - \left( \frac{r_{xw}^2 r_{zy}^2 + r_{wy}^2 r_{xz}^2 - r_{xy}^2 r_{zw}^2}{r_{zw}^4 (r_{xz}^2 r_{wy}^2 - r_{xw}^2 r_{zy}^2)} \right) \ln \frac{r_{xz}^2 r_{wy}^2}{r_{xw}^2 r_{zy}^2} \right], \quad (7)$$

as described in more detail in [38].

The expression we use for the running coupling throughout this work is

$$\alpha_{s,n_f}(r^2) = \frac{4\pi}{\beta_{0,n_f} \ln \left( \frac{4C^2}{r^2 \Lambda_{n_f}^2} \right)}, \quad (8)$$

where  $C^2$ , the so-called infrared regulator, is usually fit to data, and we fix it as  $C = 2.5$ .

Here,

$$\beta_{0,n_f} = 11 - \frac{2}{3} n_f. \quad (9)$$

$\Lambda_{n_f}^2$  is determined from the number of active flavours as [26]

$$\Lambda_{n_f-1} = (m_f)^{1 - \frac{\beta_{0,n_f}}{\beta_{0,n_f-1}}} (\Lambda_{n_f})^{\frac{\beta_{0,n_f}}{\beta_{0,n_f-1}}}, \quad (10)$$

where the active flavours are given by the dipole size and the quark mass  $m_f$  as

$$r^2 < \frac{4C^2}{m_f^2}. \quad (11)$$

We consider up to 5 active flavours,  $N_C = 3$ , and set  $m_f = 0.1 \text{ GeV}/c^2$  for the light quarks, and  $m_c = 1.3 \text{ GeV}/c^2$ ,  $m_b = 4.5 \text{ GeV}/c^2$  for the massive quarks. To fix the value of

the  $\Lambda_5$ , we use the measured value of  $\alpha_s(M_Z) = 0.1189 \pm 0.0017$  at the mass of the  $Z^0$  boson  $M_Z = 91.18 \text{ GeV}/c^2$  [49]. From a certain dipole size, namely when

$$r^2 \geq \frac{4C^2}{\Lambda_3^2} \exp \left[ -\frac{4\pi}{\beta_{0,3}\alpha_{s,0}} \right], \quad (12)$$

the growth of the coupling constant needs to be frozen at a fixed value  $\alpha_{s,0}$  [26, 50]. In the scope of this work, the choice is  $\alpha_{s,0} = 1$ .

The initial condition we chose for the evolution combines the Gaussian shape of the proton profile with the GBW dependence for the behaviour of the scattering amplitude as

$$N(r, b, Y = 0) = 1 - \exp \left( -\frac{1}{2} \frac{Q_{s,0}^2}{4} r^2 T(b_{q_1}, b_{q_2}) \right), \quad (13)$$

where  $b_{q_i}$  are the impact parameters of the quark and anti-quark forming the dipole and

$$T(b_{q_1}, b_{q_2}) = \left[ \exp \left( -\frac{b_{q_1}^2}{2B_G} \right) + \exp \left( -\frac{b_{q_2}^2}{2B_G} \right) \right]. \quad (14)$$

Two free parameters are required here: the saturation scale at  $Y = 0$ ,  $Q_s^2, 0$  and  $B_G$ , defining the size of the proton [45]. We set as  $Q_{s,0}^2 = 0.38 \text{ GeV}^2$  and  $B_G = 3.8 \text{ GeV}^{-2}$ .

## B. The CI BK equation

The CI BK equation, whose solutions are shown below to compare with the NLO solutions, reads

$$\partial_Y N_{xy} = \int d^2z K_{\text{CI}} \left[ N_{xz} + N_{zy} - N_{xy} - N_{xz} N_{zy} \right], \quad (15)$$

and the collinearly improved kernel is

$$K_{\text{CI}} = \frac{\bar{\alpha}_s}{2\pi} \frac{r_{xy}^2}{r_{xz}^2 r_{zy}^2} \left( \frac{r_{xy}^2}{\min(r_{xz}^2, r_{zy}^2)} \right)^{\pm \bar{\alpha}_s A_1} \frac{J_1(2\sqrt{\bar{\alpha}_s} |\rho^2|)}{\sqrt{\bar{\alpha}_s} |\rho^2|}. \quad (16)$$

Here, the exponent is positive, if  $r_{xy}^2 < \min(r_{xz}^2, r_{zy}^2)$ , otherwise the negative sign is used.

## III. SOLVING THE EQUATION

The numerical approach to solving the NLO BK equation is based on Euler's method (the Runge-Kutta method of the first order). This is because the 4-th order Runge-Kutta method is not applicable for the next-to-leading BK equation in the form used throughout our previous work (see [47, 51]) and the numerical precision is not affected by this change.



In the past works solving the BK equation considering only the dependence on the dipole size, it was advantageous to align the grid of the integration variable  $\vec{r}_{xz}$  with the grid sampling the scattering amplitude  $N(r_{xy})$ . During the evolution calculation, the values  $N(r_{xy})$ ,  $N(r_{xz})$  and  $N(r_{zy})$  are needed and having these grids aligned, one only needs to interpolate the latter, gaining a calculation speed-up.

However, this advantage drops out when including the impact-parameter dependence, as one rarely comes across a combination of the dipole size  $\vec{r}_{xz}$  and impact parameter  $\vec{b}_{xz}$  such that both coincide with the pre-calculated grid. It is therefore better to split the grids for sampling and integration altogether. This offers a significant improvement in the numerical calculation since one can tune the grids independently, to optimise for both precision and calculation speed at the cost of keeping track of the additional parameters.

Throughout this work, a logarithmic grid is used to sample the dipole amplitude in dipole size  $r$  and impact parameter  $b$ , while in rapidity  $Y$  it is sampled linearly. For the integration grids, polar coordinates are used, linear in angle and logarithmic in radius.

Although the dipole amplitude is in principle restricted to  $N(Y, r, b) \in [0, 1]$ , rounding errors and small imprecisions can cause an under- or overflow of these bounds during the calculation. Since the origin of these errors is purely numerical, such values are set to 0 or 1, correspondingly.

Several terms in the denominator of the NLO kernel are divergent when  $r_{xz}^2 r_{wy}^2 = r_{xw}^2 r_{zy}^2$ , presenting a potential numerical problem. This typically leads to the introduction of ad hoc cut-off parameters to manually tame the large contributions. We were able to avoid this altogether and accept arbitrarily large kernel values throughout the calculation. The only exception is the unlikely event of hitting one of the aforementioned divergent points, in this case, the contribution of this point is naturally set to 0.

This level of numerical stability was achieved by introducing a relative offset of all the grids sampling the transverse plane in Fig. 1. The integration polar grids are displaced as shown in Fig. 8 to avoid symmetrical configurations (for more details see Appendix A).

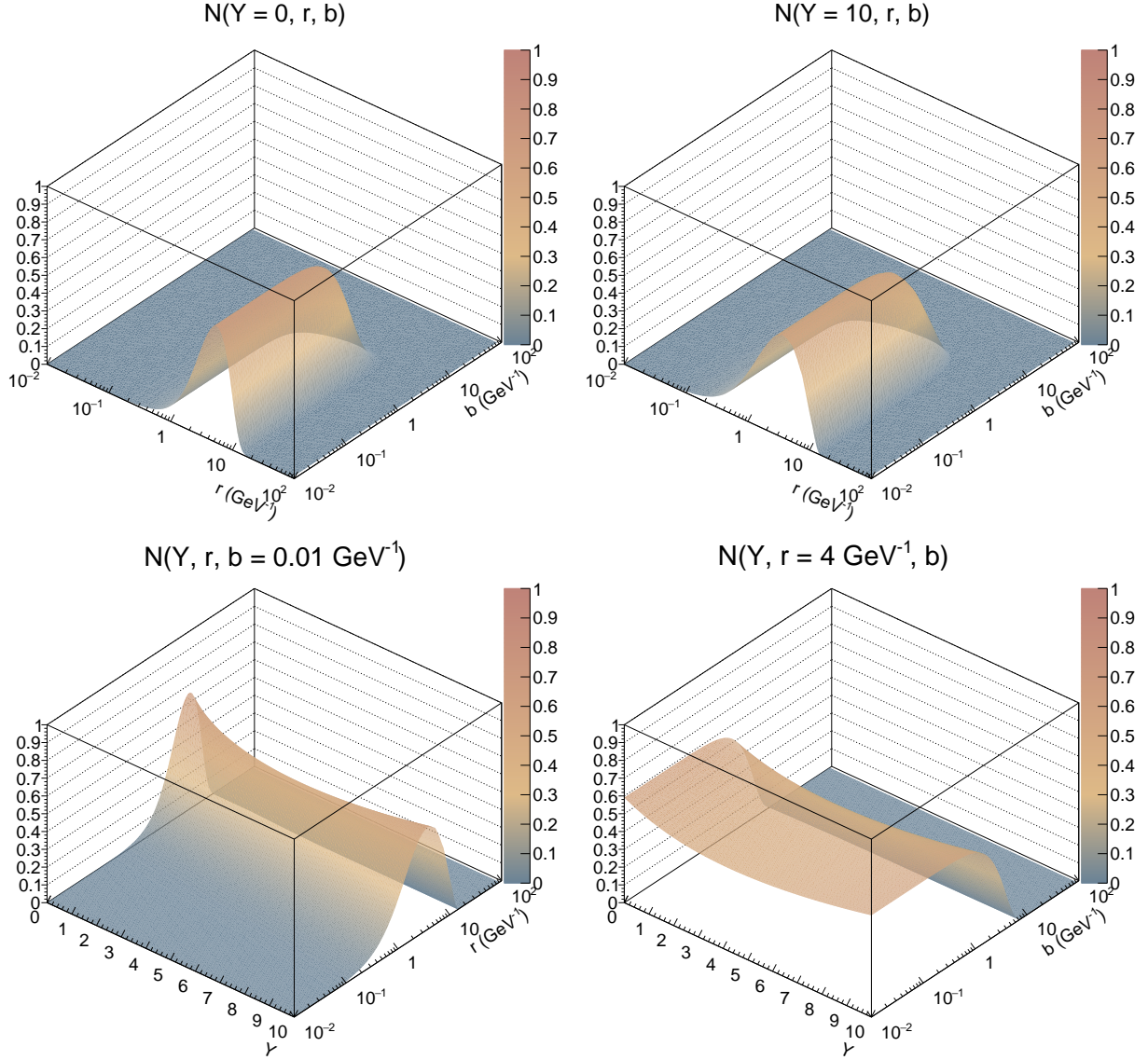


FIG. 2. The evolution of dipole scattering amplitude  $N(Y, r, b)$  according to the NLO BK equation is shown at two fixed values of rapidity in the top panels:  $Y = 0$  (top left), and  $Y = 10$  (top right). A detailed view of the rapidity evolution on  $r$  and  $b$  for fixed representative values of  $b = 0.01 \text{ GeV}^{-1}$  and  $r = 4 \text{ GeV}^{-1}$  is shown in the bottom left, respectively right, panels.

## IV. SOLUTIONS TO THE BK EQUATION AT NLO

### A. Evolution of the dipole scattering amplitude

The evolution of  $N(Y, r, b)$  according to the NLO BK equation, from the initial condition  $Y = 0$  to  $Y = 10$ , is shown in the upper panels of Fig. 2. The evolution is very smooth with

the dipole amplitude retaining its shape as the rapidity increases. The evolution in  $r$  of the forward wavefront is clearly seen, while the backward front changes very little. The shape as a function of the dipole size shows little dependence on the impact parameter for small and moderate values of  $b$ , while there is a mild evolution on the support at large impact parameters.

To have a more detailed picture of the evolution, the lower two panels of Fig. 2 show the rapidity dependence of the evolution in  $r$  (bottom left) and  $b$  (bottom right) for fixed representative values of  $b = 0.01 \text{ GeV}^{-1}$  and  $r = 4 \text{ GeV}^{-1}$ , respectively. In both cases one can observe that the maximum of the amplitude first decreases, and then after a few rapidity units it increases. This behaviour, along with the observation that the value of the dipole scattering amplitude does not reach one, has interesting implications for the definition of the saturation scale discussed in Sec. IV C. Figure 3 shows  $r$  and  $b$  slices of the scattering dipole

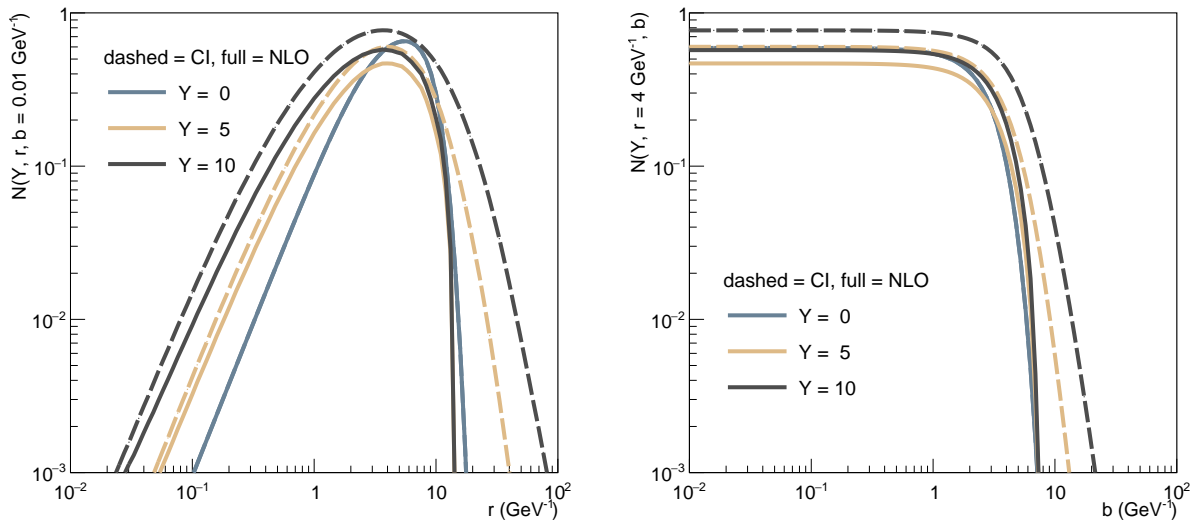


FIG. 3. Comparison of the dipole scattering amplitude obtained within the collinearly improved (CI) and next-to-leading order (NLO) evolutions for a fixed value of  $b = 0.01 \text{ GeV}^{-1}$  (left) and  $r = 4 \text{ GeV}^{-1}$  (right). Three different values of rapidity are shown.

amplitudes for the CI and NLO BK equations at three values of rapidity,  $Y = 0, 5, 10$ , at fixed values of  $b = 0.01 \text{ GeV}^{-1}$  and  $r = 4 \text{ GeV}^{-1}$ , respectively. The behaviour described before is easier to see in this figure: the forward wavefront advances faster than the backward one, and the maximum value of  $N$  first decreases and then increases with the behaviour independent of the impact parameter for most of the range. The figure also compares the evolution at

NLO with that of the CI equation. At NLO the evolution is substantially slower than for CI. This behaviour applies for both fronts in  $r$  as well as for the decay at large values of the impact parameter.

An important observation from the right panel of Fig. 3, is that for the NLO evolution, there are no Coulomb tails. This behaviour is puzzling. We expected, that as in the case of CI evolution, the Coulomb tails would be suppressed with respect to what was found using previous kernels [39]. For the case of CI solutions, the suppression was explained [44] by the confluence of two contributions: the CI kernel that suppresses large daughter dipoles and the chosen initial condition that does not include Coulomb tails. A similar conclusion was found in Ref. [46] where it was clarified that this is likely a transient behaviour and the tails would reappear at larger rapidities, as commonly expected, see e.g. Ref. [52]. The initial condition chosen for the solution of the NLO BK equation is similar to what was used before and, as seen above, the NLO evolution is slower, so smaller tails were expected. There, however, seems to be none. At the moment, we do not understand this behaviour. Our current interpretation is that the tails are indeed smaller and that our method for the numerical solution of the NLO BK equation tends to suppress them even more. One argument against this latter hypothesis is that the exact same code is used to solve the CI BK equation and in this case the Coulomb tails, though suppressed are observed. As the numerical exploration of what could be happening is quite slow, we decided just to report the observation and discuss more quantitatively the possible origin somewhere else. Note that otherwise, the obtained solutions show no strange or unstable behaviour at all.

## B. Anomalous dimension and evolution speed

Here, we present two important characteristics of the evolution of the dipole amplitude: the anomalous dimension and the evolution speed. In both cases, the behaviour of the NLO BK equation solutions is further compared to that of the CI case.

The anomalous dimension is defined as

$$\gamma(Y, r, b) = \frac{\partial \ln N(Y, r, b)}{\partial \ln r^2}, \quad (17)$$

and it is shown in Fig. 4 as a function of the dipole size  $r$  at a representative value of the impact parameter. The anomalous dimension is flat for the NLO dipole amplitudes for

most of the range in dipole sizes. For large dipoles, the anomalous dimension decreases quite rapidly. Upon evolution, the anomalous dimension seems to slightly decrease its value at medium and small dipole sizes, but the numerical fluctuations are large compared to this effect. The anomalous dimension for the CI case shows the same behaviour. At large values of the dipole size (above  $10 \text{ GeV}^{-1}$ ) the shape of the anomalous dimension is markedly different between both cases. This is related to the fact that for the NLO evolution, there is almost no change for the backward front of the dipole amplitude, as mentioned above.

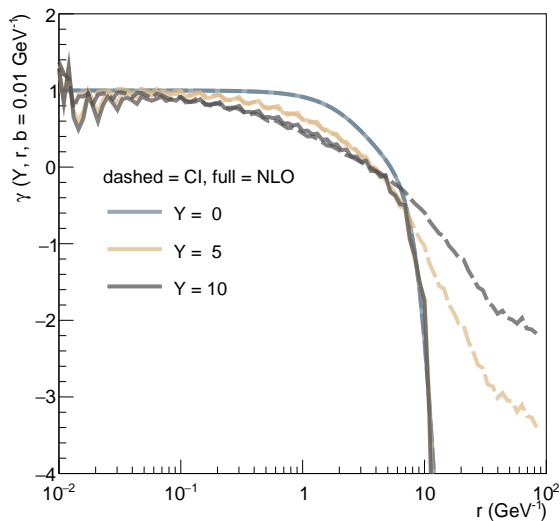


FIG. 4. Anomalous dimension  $\gamma$  as a function of the dipole size at a representative impact parameter  $b = 0.01 \text{ GeV}^{-1}$  and three points of the rapidity evolution. Dashed curves show the leading order results (CI), while the NLO results are plotted in full curves.

Another important characteristic of the solutions to the BK equation is the evolution speed:  $\partial_Y N(Y, r, b)$ , which is shown in Fig. 5 for a fixed impact parameter  $b = 0.01 \text{ GeV}^{-1}$  and three different rapidities. The evolution speed for dipole sizes above around  $2 \text{ GeV}^{-1}$  is negative and at even larger dipole sizes show a different behaviour for CI and NLO amplitudes. At sizes below around  $2 \text{ GeV}^{-1}$ , that is for the forward wavefront, the evolution speed is noticeably slower for the NLO evolution with respect to the CI case. To demonstrate that this behaviour is similar at other impact parameters, we show in Fig. 6 the evolution speed at rapidity 10 as a function of both the dipole size and the impact parameter for CI (left) and NLO (right) dipole amplitudes.

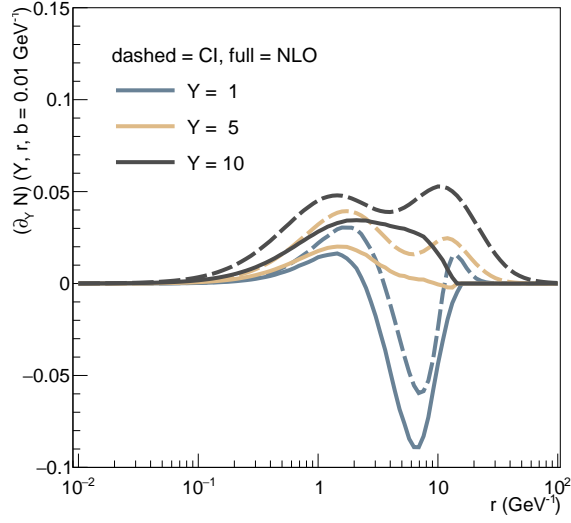


FIG. 5. The evolution speed as a function of the dipole size  $r$  at a representative impact parameter  $b = 0.01 \text{ GeV}^{-1}$  and three steps of the rapidity evolution. The CI BK corresponds to the dashed curves, the NLO BK is shown in full.

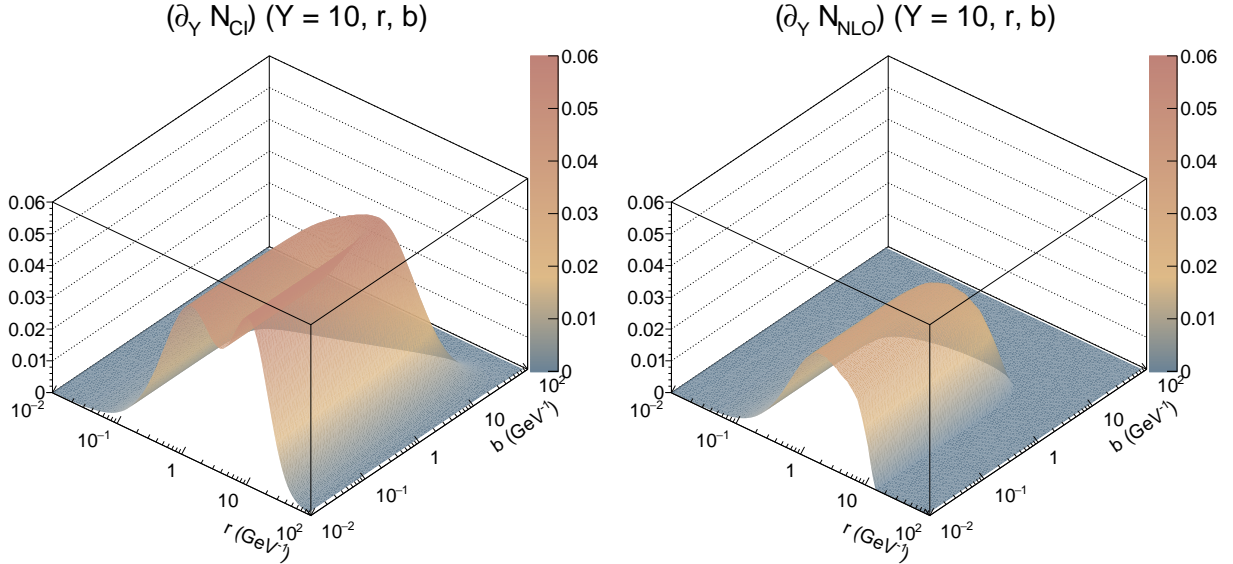


FIG. 6. The evolution speed as a function of the dipole size  $r$  and impact parameter  $b$  at rapidity  $Y = 10$  for the CI BK (left panel) and the NLO BK (right panel).

### C. Saturation scale

Now, we turn to the saturation scale  $Q_s = Q_s(Y, b)$  defined as

$$N(Y, r = 1/Q_s, b) = \kappa, \quad (18)$$

and its dependence on the impact parameter and rapidity. The constant  $\kappa$  is of the order of unity. Two values for  $\kappa$  have been traditionally used in the past: 0.5 or  $1 - \exp(-1/2) \approx 0.4$ . Looking again at the upper left panel of Fig. 3 we see that there are rapidities for which the maximum of the amplitude does not reach 0.5. This would produce a situation where the saturation scale is defined at the initial condition, then there is no saturation scale, and finally, at larger rapidities, the saturation would again appear. To avoid this we decided to use  $\kappa = 0.4$ .

The behaviour of the saturation scale in CI and NLO BK is shown in Fig. 7. For impact parameters below around  $1 \text{ GeV}^{-1}$ , the saturation scale is constant in both cases. The dependence of  $Q_s$  on rapidity is steeper for the CI case, which is expected, given the observations discussed in the previous section. For  $Y = 10$  the saturation scale at small to moderate impact parameters reaches a value of  $0.7 \text{ GeV}$  for the NLO case while it is above  $1 \text{ GeV}$  for CI, after having started in both cases at a value of  $0.4 \text{ GeV}$  at the initial rapidity.

## V. SUMMARY

This paper presents the first stable solution of the next-to-leading order BK equation including the dependence on the dipole size as well as on the impact parameter. We described the numerical method allowing for a stable solution, namely the proper choice of misaligned integration grids. This way the contribution of divergent kernel points can be minimised and the only necessary numerical intervention is to hard restrict the dipole amplitude values  $N(Y, r, b) \in [0, 1]$ .

The solution to the leading-order equation BK equation with collinearly improved kernel (CI) was shown to compare it with the NLO evolution. Overall, the NLO evolution is slower and suppresses the contribution of both large dipoles and large impact parameters. The almost absolute suppression of the Coulomb tails, is, however, stronger than expected and remains to be further addressed.

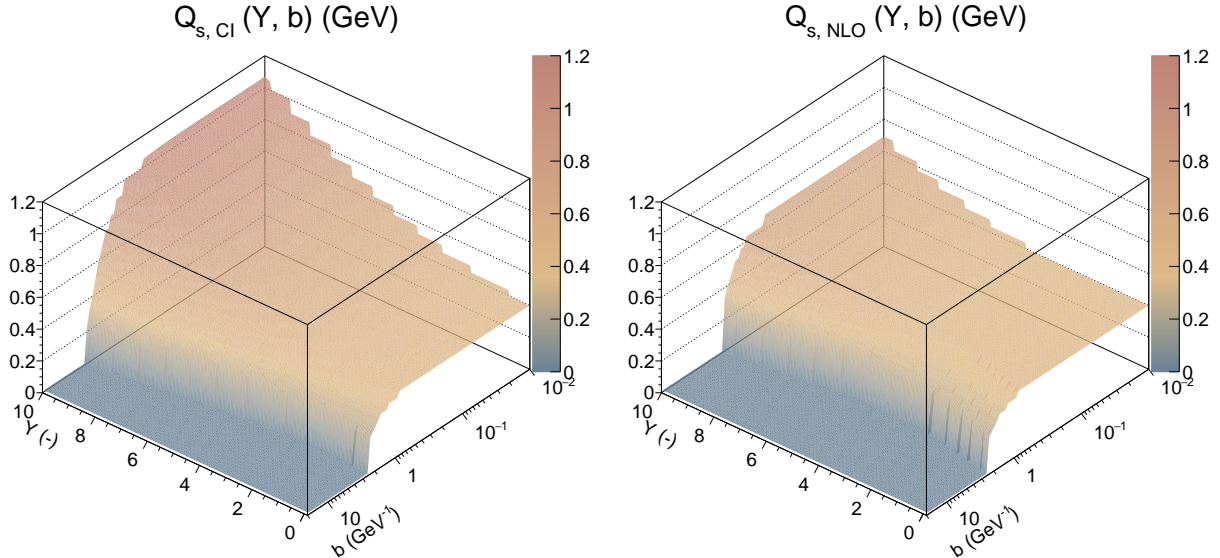


FIG. 7. The evolution of the saturation scale for the solutions of the CI (left) and NLO (right) BK equations from  $Y = 0$  to  $Y = 10$  is shown as a function of the dipole size and the impact parameter.

To characterize the amplitude evolution, the anomalous dimension and evolution speed are plotted and discussed from the perspective of both the NLO and CI BK equations. The evolution speed of the NLO BK is overall smaller than in the CI case and as the rapidity increases, the NLO anomalous dimension is shown to be more stable.

Finally, the evolution of the saturation scale is compared again for the NLO and CI BK equation, quantifying the different regions in which the saturation effects are considered to take effect.

These results present a breakthrough in numerical solutions of the BK equation, paving the way to its application to compute observables to search for saturation with next-to-leading order precision.

**Data availability:** The scattering amplitudes are publicly available at the CERN-based open repository ZENODO [53].

## ACKNOWLEDGMENTS

This work was partially funded by the Czech Science Foundation (GAČR), project No. 22-27262S. Marek Matas was furthermore supported by the CTU Mobility Project MSCA-



### Appendix A: Numerical solution of the BK equation at next-to-leading order

Here we summarize the numerical approach to solving the NLO BK equation. Using Simpson's integration method enabled good tracking of points causing the numerical instabilities in the BK equation, allowing us to pinpoint the main problem to the overly symmetric sampling of the integration space.

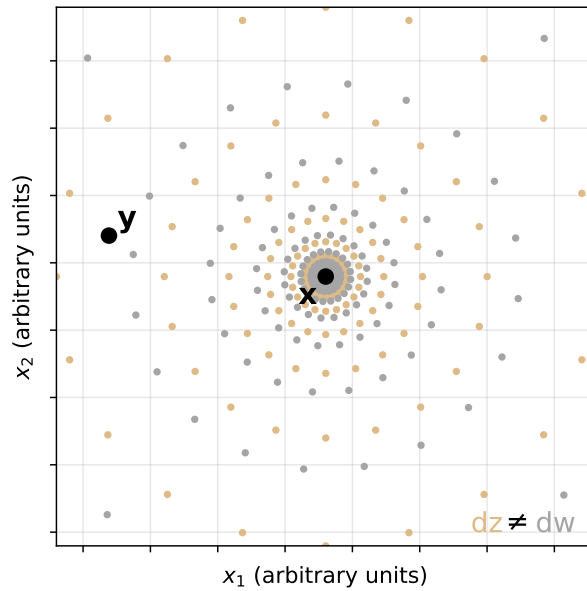


FIG. 8. Schematic structure of the integration grids in the transverse plane, same as in Fig. 1. Both grids (in  $dz$  and  $dw$ ) are polar with logarithmic spacing in the radial coordinate, centred around one of the quarks. To ensure uniform sampling of the integrand with less emphasis on the high-symmetry divergent points, they are offset w.r.t. each other and the sampling grid. The grids in this picture have been adjusted for better clarity and do not have the actual number of points.

The key ingredient for overcoming the instability was therefore identified as displacing the sampling (the points in the transverse plane in which the quark and antiquark of the mother dipole are placed during the calculation) and both integration (the points in the transverse plane in which the emerging gluons, vertices of the daughter dipoles, are placed during the calculation) grids as shown in Fig. 8. This way, quarks and gluons not only never emerge at the same point (giving zero dipole sizes), but rarely hit a symmetrical configuration, in

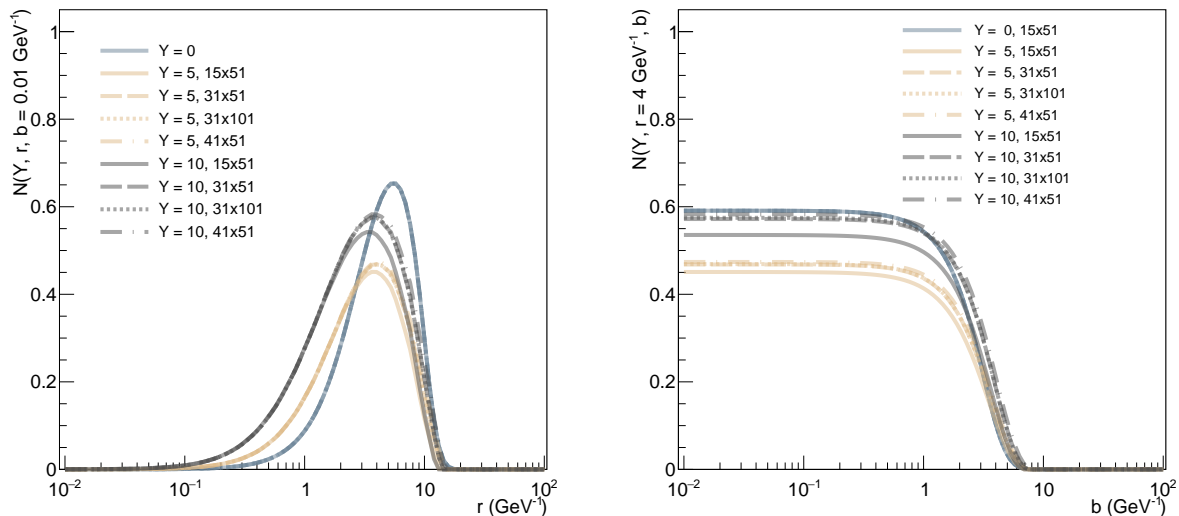


FIG. 9. The dipole amplitude at various stages of the evolution using  $n_a \times n_r$  points in integration grids, where  $n_a$  is the number of angular points and  $n_r$  is the number of radial points. Clearly the  $31 \times 51$  setup is fine enough for a convergent solution.

which e.g.  $r_{xz}^2 r_{wy}^2 - r_{xw}^2 r_{zy}^2 = 0$ . Omitting these (and adjacent) configurations, in which the kernels diverge (analytically or numerically because of the limited numerical precision) gives a solid numerical set-up to solve the NLO BK equation. Furthermore, Fig. 9 shows the stability of the solution by varying the computational set-up.

The integration grids are polar with linear sampling in the angular variable  $\varphi$  and logarithmic in the radial  $r$ , centred at the quark position  $x$  (the left quark in Fig. 1). The displacement then corresponds to shifting the initial and final grid point somewhere close to the middle of the other grid (a place somewhere close to the middle is chosen by dividing the interval by  $\sqrt{3}$ ), such that the divergence-causing symmetry remains unrecovered and equidistantly, in both the linear and logarithmic sense, sampling the resulting interval, as depicted in Fig. 8. The shifting values were chosen heuristically and are listed in Tab. I.

- 
- [1] F. D. Aaron *et al.* (H1, ZEUS), Combined Measurement and QCD Analysis of the Inclusive  $e^+p$  Scattering Cross Sections at HERA, *JHEP* **01**, 109, arXiv:0911.0884 [hep-ex].
  - [2] L. V. Gribov, E. M. Levin, and M. G. Ryskin, Semihard Processes in QCD, *Phys. Rept.* **100**,

<b>sampling grid</b>	<b>value, sampling</b>
rapidity $Y$	lin, [0,10], 201 points
dipole size $r$	log, [ $10^{-2}$ , $10^2$ ], 101 points
impact parameter $b$	log, [ $10^{-2}$ , $10^2$ ], 101 points
<b>integration grid (z) value, sampling</b>	
radius $r_z$	log, [ $1.1 \cdot 10^{-2}$ , $1.1 \cdot 10^2$ ], 51 points
angle $\varphi_z$	lin, [0.100, 6.383], 31 points
<b>integration grid (w) value, sampling</b>	
radius $r_w$	log, [ $1.21 \cdot 10^{-2}$ , $1.21 \cdot 10^2$ ], 51 points
angle $\varphi_w$	lin, [0.217, 6.500], 31 points

TABLE I. Values of the parameters used in the convergent Simpson-based calculation. Values of radius and impact parameter are in the units of  $\text{GeV}^{-1}$ , angular variables are in rad, rapidity and number of samples are dimensionless.

- 1 (1983).
- [3] A. H. Mueller and J.-w. Qiu, Gluon Recombination and Shadowing at Small Values of  $x$ , Nucl. Phys. B **268**, 427 (1986).
- [4] A. Morreale and F. Salazar, Mining for Gluon Saturation at Colliders, Universe **7**, 312 (2021), arXiv:2108.08254 [hep-ph].
- [5] J. G. Contreras and J. D. Tapia Takaki, Ultra-peripheral heavy-ion collisions at the LHC, Int. J. Mod. Phys. A **30**, 1542012 (2015).
- [6] S. R. Klein and H. Mäntysaari, Imaging the nucleus with high-energy photons, Nature Rev. Phys. **1**, 662 (2019), arXiv:1910.10858 [hep-ex].
- [7] S. Acharya *et al.* (ALICE), The ALICE experiment: a journey through QCD, Eur. Phys. J. C **84**, 813 (2024), arXiv:2211.04384 [nucl-ex].
- [8] A. Accardi *et al.*, Electron Ion Collider: The Next QCD Frontier: Understanding the glue that binds us all, Eur. Phys. J. A **52**, 268 (2016), arXiv:1212.1701 [nucl-ex].
- [9] R. Abdul Khalek *et al.*, Science Requirements and Detector Concepts for the Electron-Ion Collider: EIC Yellow Report, Nucl. Phys. A **1026**, 122447 (2022), arXiv:2103.05419 [physics.ins-det].
- [10] Y. V. Kovchegov and E. Levin, *Quantum Chromodynamics at High Energy*, Vol. 33 (Oxford

- University Press, 2013).
- [11] F. Gelis, E. Iancu, J. Jalilian-Marian, and R. Venugopalan, The Color Glass Condensate, *Ann. Rev. Nucl. Part. Sci.* **60**, 463 (2010), arXiv:1002.0333 [hep-ph].
  - [12] I. Balitsky, Operator expansion for high-energy scattering, *Nucl. Phys. B* **463**, 99 (1996), arXiv:hep-ph/9509348.
  - [13] J. Jalilian-Marian, A. Kovner, A. Leonidov, and H. Weigert, The BFKL equation from the Wilson renormalization group, *Nucl. Phys. B* **504**, 415 (1997), arXiv:hep-ph/9701284.
  - [14] J. Jalilian-Marian, A. Kovner, A. Leonidov, and H. Weigert, The Wilson renormalization group for low x physics: Towards the high density regime, *Phys. Rev. D* **59**, 014014 (1998), arXiv:hep-ph/9706377.
  - [15] J. Jalilian-Marian, A. Kovner, and H. Weigert, The Wilson renormalization group for low x physics: Gluon evolution at finite parton density, *Phys. Rev. D* **59**, 014015 (1998), arXiv:hep-ph/9709432.
  - [16] A. Kovner, J. G. Milhano, and H. Weigert, Relating different approaches to nonlinear QCD evolution at finite gluon density, *Phys. Rev. D* **62**, 114005 (2000), arXiv:hep-ph/0004014.
  - [17] H. Weigert, Unitarity at small Bjorken x, *Nucl. Phys. A* **703**, 823 (2002), arXiv:hep-ph/0004044.
  - [18] E. Iancu, A. Leonidov, and L. D. McLerran, Nonlinear gluon evolution in the color glass condensate. 1., *Nucl. Phys. A* **692**, 583 (2001), arXiv:hep-ph/0011241.
  - [19] E. Iancu, A. Leonidov, and L. D. McLerran, The Renormalization group equation for the color glass condensate, *Phys. Lett. B* **510**, 133 (2001), arXiv:hep-ph/0102009.
  - [20] E. Ferreira, E. Iancu, A. Leonidov, and L. McLerran, Nonlinear gluon evolution in the color glass condensate. 2., *Nucl. Phys. A* **703**, 489 (2002), arXiv:hep-ph/0109115.
  - [21] Y. V. Kovchegov, Small x F(2) structure function of a nucleus including multiple pomeron exchanges, *Phys. Rev. D* **60**, 034008 (1999), arXiv:hep-ph/9901281.
  - [22] Y. V. Kovchegov, Unitarization of the BFKL pomeron on a nucleus, *Phys. Rev. D* **61**, 074018 (2000), arXiv:hep-ph/9905214.
  - [23] J. L. Albacete, Particle multiplicities in Lead-Lead collisions at the LHC from non-linear evolution with running coupling, *Phys. Rev. Lett.* **99**, 262301 (2007), arXiv:0707.2545 [hep-ph].
  - [24] J. L. Albacete and Y. V. Kovchegov, Solving high energy evolution equation including running

- coupling corrections, *Phys. Rev. D* **75**, 125021 (2007), arXiv:0704.0612 [hep-ph].
- [25] J. L. Albacete, N. Armesto, J. G. Milhano, and C. A. Salgado, Non-linear QCD meets data: A Global analysis of lepton-proton scattering with running coupling BK evolution, *Phys. Rev. D* **80**, 034031 (2009), arXiv:0902.1112 [hep-ph].
- [26] J. L. Albacete, N. Armesto, J. G. Milhano, P. Quiroga-Arias, and C. A. Salgado, AAMQS: A non-linear QCD analysis of new HERA data at small-x including heavy quarks, *Eur. Phys. J. C* **71**, 1705 (2011), arXiv:1012.4408 [hep-ph].
- [27] E. Iancu, J. D. Madrigal, A. H. Mueller, G. Soyez, and D. N. Triantafyllopoulos, Resumming double logarithms in the QCD evolution of color dipoles, *Phys. Lett. B* **744**, 293 (2015), arXiv:1502.05642 [hep-ph].
- [28] E. Iancu, J. D. Madrigal, A. H. Mueller, G. Soyez, and D. N. Triantafyllopoulos, Collinearly-improved BK evolution meets the HERA data, *Phys. Lett. B* **750**, 643 (2015), arXiv:1507.03651 [hep-ph].
- [29] G. Beuf, Dipole factorization for DIS at NLO: Loop correction to the  $\gamma_{T,L}^* \rightarrow q\bar{q}$  light-front wave functions, *Phys. Rev. D* **94**, 054016 (2016), arXiv:1606.00777 [hep-ph].
- [30] G. Beuf, Dipole factorization for DIS at NLO: Combining the  $q\bar{q}$  and  $q\bar{q}g$  contributions, *Phys. Rev. D* **96**, 074033 (2017), arXiv:1708.06557 [hep-ph].
- [31] G. Beuf, T. Lappi, and R. Paatelainen, Massive quarks in NLO dipole factorization for DIS: Longitudinal photon, *Phys. Rev. D* **104**, 056032 (2021), arXiv:2103.14549 [hep-ph].
- [32] G. Beuf, T. Lappi, and R. Paatelainen, Massive Quarks at One Loop in the Dipole Picture of Deep Inelastic Scattering, *Phys. Rev. Lett.* **129**, 072001 (2022), arXiv:2112.03158 [hep-ph].
- [33] G. Beuf, T. Lappi, and R. Paatelainen, Massive quarks in NLO dipole factorization for DIS: Transverse photon, *Phys. Rev. D* **106**, 034013 (2022), arXiv:2204.02486 [hep-ph].
- [34] H. Mäntysaari and J. Penttala, Complete calculation of exclusive heavy vector meson production at next-to-leading order in the dipole picture, *JHEP* **08**, 247, arXiv:2204.14031 [hep-ph].
- [35] G. Beuf, T. Lappi, H. Mäntysaari, R. Paatelainen, and J. Penttala, Diffractive deep inelastic scattering at NLO in the dipole picture, *JHEP* **05**, 024, arXiv:2401.17251 [hep-ph].
- [36] I. Balitsky and G. A. Chirilli, Next-to-leading order evolution of color dipoles, *Phys. Rev. D* **77**, 014019 (2008), arXiv:0710.4330 [hep-ph].
- [37] T. Lappi and H. Mäntysaari, Direct numerical solution of the coordinate space Balitsky-Kovchegov equation at next to leading order, *Phys. Rev. D* **91**, 074016 (2015),

- arXiv:1502.02400 [hep-ph].
- [38] T. Lappi and H. Mäntysaari, Next-to-leading order Balitsky-Kovchegov equation with resummation, *Phys. Rev. D* **93**, 094004 (2016), arXiv:1601.06598 [hep-ph].
  - [39] K. J. Golec-Biernat and A. M. Stasto, On solutions of the Balitsky-Kovchegov equation with impact parameter, *Nucl. Phys. B* **668**, 345 (2003), arXiv:hep-ph/0306279.
  - [40] L. Motyka and A. M. Stasto, Exact kinematics in the small  $x$  evolution of the color dipole and gluon cascade, *Phys. Rev. D* **79**, 085016 (2009), arXiv:0901.4949 [hep-ph].
  - [41] J. Berger and A. Stasto, Numerical solution of the nonlinear evolution equation at small  $x$  with impact parameter and beyond the LL approximation, *Phys. Rev. D* **83**, 034015 (2011), arXiv:1010.0671 [hep-ph].
  - [42] J. Berger and A. M. Stasto, Small  $x$  nonlinear evolution with impact parameter and the structure function data, *Phys. Rev. D* **84**, 094022 (2011), arXiv:1106.5740 [hep-ph].
  - [43] J. Berger and A. M. Stasto, Exclusive vector meson production and small- $x$  evolution, *JHEP* **01**, 001, arXiv:1205.2037 [hep-ph].
  - [44] J. Cepila, J. G. Contreras, and M. Matas, Collinearly improved kernel suppresses Coulomb tails in the impact-parameter dependent Balitsky-Kovchegov evolution, *Phys. Rev. D* **99**, 051502 (2019), arXiv:1812.02548 [hep-ph].
  - [45] D. Bendova, J. Cepila, J. G. Contreras, and M. Matas, Solution to the Balitsky-Kovchegov equation with the collinearly improved kernel including impact-parameter dependence, *Phys. Rev. D* **100**, 054015 (2019), arXiv:1907.12123 [hep-ph].
  - [46] C. Contreras, E. Levin, and R. Meneses, BFKL equation in the next-to-leading order: solution at large impact parameters, *Eur. Phys. J. C* **79**, 842 (2019), arXiv:1906.09603 [hep-ph].
  - [47] J. Cepila, J. G. Contreras, and M. Vaculciak, Solutions to the Balitsky-Kovchegov equation including the dipole orientation, *Phys. Lett. B* **848**, 138360 (2024), arXiv:2309.02910 [hep-ph].
  - [48] B. Ducloué, E. Iancu, A. H. Mueller, G. Soyez, and D. N. Triantafyllopoulos, Non-linear evolution in QCD at high-energy beyond leading order, *JHEP* **04**, 081, arXiv:1902.06637 [hep-ph].
  - [49] K. A. Olive *et al.* (Particle Data Group), Review of Particle Physics, *Chin. Phys. C* **38**, 090001 (2014).
  - [50] P. Quiroga-Arias, J. L. Albacete, N. Armesto, J. G. Milhano, and C. A. Salgado, AAMQS: a non-linear QCD description of new HERA data at small- $x$ , *J. Phys. G* **38**, 124124 (2011),

arXiv:1107.0625 [hep-ph].

- [51] J. Cepila and J. G. Contreras, Rapidity dependence of saturation in inclusive HERA data with the rcBK equation, (2015), arXiv:1501.06687 [hep-ph].
- [52] E. Gotsman and E. Levin, Large impact parameter behavior in the CGC/saturation approach: A new nonlinear equation, Phys. Rev. D **101**, 014023 (2020), arXiv:1910.11662 [hep-ph].
- [53] M. Vaculciak, Bk\_nlo\_2d, 10.5281/zenodo.14362815 (2024).